ARMY RESEARCH LABORATORY

Dynamic Analysis of Helicopter Bearingless Main Rotor With Hub Flexbeam Damage Configurations

Ki C. Kim

ARL-TR-921

January 1996

NOTICES

Destroy this report when it is no longer needed. DO NOT return it to the originator.

Additional copies of this report may be obtained from the National Technical Information Service, U.S. Department of Commerce, 5285 Port Royal Road, Springfield, VA 22161.

The findings of this report are not to be construed as an official Department of the Army position, unless so designated by other authorized documents.

The use of trade names or manufacturers' names in this report does not constitute indorsement of any commercial product.

REPORT DOCUMENTATION PAGE

Form Approved
OMB No. 0704-0188

1. AGENCY USE ONLY *(Leave blank)*	2. REPORT DATE	3. REPORT TYPE AND DATES COVERED
	January 1996	Final, May 93 - Sep 94

4. TITLE AND SUBTITLE

Dynamic Analysis of Helicopter Bearingless Main Rotor With Hub Flexbeam Damage Configurations

5. FUNDING NUMBERS

PR: 1L162618AH80

6. AUTHOR(S)

Ki C. Kim

7. PERFORMING ORGANIZATION NAME(S) AND ADDRESS(ES)

U.S. Army Research Laboratory
ATTN: AMSRL-SL-BA
Aberdeen Proving Ground, MD 21005-5068

8. PERFORMING ORGANIZATION REPORT NUMBER

ARL-TR-921

9. SPONSORING/MONITORING AGENCY NAMES(S) AND ADDRESS(ES)

10.SPONSORING/MONITORING AGENCY REPORT NUMBER

11. SUPPLEMENTARY NOTES

12a. DISTRIBUTION/AVAILABILITY STATEMENT

Approved for public release; distribution is unlimited.

12b. DISTRIBUTION CODE

13. ABSTRACT *(Maximum 200 words)*

This report documents a dynamic analysis of a helicopter bearingless main rotor system with damaged hub flexbeam configurations. The analysis was performed using a comprehensive helicopter aeroelastic code based on finite element/blade element theory. The bearingless main rotor (BMR) system, including flexbeams, torque tubes, and main rotor blades, is modeled as a number of elastic beam finite elements, wherein each beam element undergoes flap bending, lag bending, elastic twist, and axial deflections. Aerodynamic forces on rotor blades are calculated using quasisteady aerodynamic theory with a linear in-flow model. Flexbeam ballistic damage is simulated by changes in the span-wise distribution of the mass, bending and torsional stiffness of flexbeam element. Results are first calculated for a soft in-plane, five-bladed, bearingless rotor, with an undamaged (baseline) configuration. Results are then calculated for this rotor system with damage representation. The effects of this damage on rotor and helicopter system performances are determined in terms of blade modal shapes and frequencies, rotor system aeroelastic response and loads variations. Ballistic damage to the hub flexbeam can significantly affect the dynamic behavior of the bearingless rotor system.

14. SUBJECT TERMS	15. NUMBER OF PAGES
helicopters, dynamics, aerodynamics, vibration, finite element method	34
	16. PRICE CODE

17. SECURITY CLASSIFICATION OF REPORT	18. SECURITY CLASSIFICATION OF THIS PAGE	19. SECURITY CLASSIFICATION OF ABSTRACT	20. LIMITATION OF ABSTRACT
UNCLASSIFIED	UNCLASSIFIED	UNCLASSIFIED	UL

INTENTIONALLY LEFT BLANK.

Table of Contents

INTENTIONALLY LEFT BLANK.

List of Figures

INTENTIONALLY LEFT BLANK.

I. Introduction

The bearingless main rotor is the design configuration for the Army's next generation combat helicopter; it offers design simplicity (fewer parts), weight reduction, better maintenance, and more control power and maneuverability. A bearingless rotor is a special case of a hingeless rotor, in which the pitch bearing as well as the flap and lag hinges are eliminated (see Figure 1). Pitch control from the pitch link to the main blade is transmitted via a torsionally stiff torque tube. This in turn twists a torsionally soft flexbeam, which functions effectively as a pitch bearing. The flexbeam is actually a major component of the bearingless rotor design; it carries the centrifugal load and allows for the blade flap, lead lag, and twist motions. There is, however, a lack of vulnerability information for the flight-critical flexbeam element attributable to ballistic damage mechanisms. In addition, the effects of flexbeam ballistic damage on the rotor and helicopter system's performance are not adequately understood.

The objective of the present research is to analytically investigate rotor and aircraft performance effects caused by flexbeam damage. The present investigation was performed using the University of Maryland advanced rotorcraft code (UMARC) [1]. The bearingless main rotor (BMR) system, including flexbeams, torque tubes, and main rotor blades, was modeled as a number of elastic beam finite elements, wherein each beam element undergoes flap bending, lag bending, elastic twist, and axial deflections. Flexbeam ballistic damage was simulated as changes in the span-wise distribution of the mass, bending and torsional stiffness of flexbeam element.

Results are first calculated for an advanced five-bladed BMR with a baseline (undamaged) configuration. Results then are calculated for this rotor system with representative levels of ballistic damage to the hub flexbeam. The effects of this damage on this helicopter's performance are determined in terms of blade modal shapes and frequencies, rotor system dynamic response and loads.

In the context of the U.S. Army Research Laboratory's (ARL) process structure for analyzing combat system vulnerability, this study and its associated engineering-based methods address the mapping from Level 2, the Target Component Damage State, to Level 3, the Target Capability State (i.e., $O_{2,3}$ mapping); other levels include 1, Threat/Target Initial Conditions and 4, Target Combat Utility. See Reference 2 for more details. A significant feature of this process is that at each level (or space), distinct, measurable

information is available, defining the threat-target encounter and vulnerability/lethality outcome. Here, for example, physical and structural factors defining hub flexbeam damage (Level 2) are mapped via engineering methods into parameters that define the rotor and helicopter system's functional capability (Level 3); all the defining terms are explicit and measurable through experimentation. Application of these and other engineering analysis tools to the vulnerability/lethality process structure will occur largely through implementation in the degraded states vulnerability methodology for level $O_{2,3}$ mapping now being developed for aircraft targets at ARL.

II. Nomenclature

C_w	Helicopter weight coefficient, $W/\pi R^2\rho(\Omega R)^2$.
c_m	Blade mean chord, *ft.*
EI_y	Flap-wise bending stiffness, $lb-in^2$.
EI_z	Chord-wise bending stiffness, $lb-in^2$.
GJ	Effective sectional torsional stiffness, $lb-in^2$.
l_i	Length of the ith beam element, *ft.*
m	Blade section mass, *slug.*
m_o	Reference blade section mass, *slug.*
N_b	Number of blades.
$\mathbf{q}$	Global displacement vector.
R	Blade radius, *ft.*
T	Rotor thrust, *lb.*
u	Blade displacement in the axial direction, *ft.*
v	Blade displacement in the lead lag direction, *ft.*
V	Helicopter forward speed, *ft/sec.*
w	Blade displacement in the flap-wise direction, *ft.*
W	Helicopter gross weight, *lb.*
α	Blade section angle of attack, *rad.*
α_s	Longitudinal shaft tilt relative to wind axis, *rad.*
β_0	Rotor coning angle, *rad.*
β_{1s}, β_{1c}	Lateral and longitudinal rotor disk tilt angle, respectively, *rad.*

θ_{1c}, θ_{1s}	Lateral and longitudinal cyclic trim inputs, respectively, *rad.*
$\theta_{.75}$	Collective blade pitch at 75% radius, *rad.*
μ	Advance ratio, $V/\Omega R$.
σ	Rotor solidity ratio, $N_b c_m/\pi R$.
$\hat{\phi}$	Blade twist, *rad/ft.*
ϕ_s	Lateral shaft tilt, *rad.*
ρ	Air density, $slug/ft^3$.
Ω	Rotor rotational speed, *rad/sec.*
θ_{tr}	Tail rotor collective control setting, *rad.*

III. Formulation and Analysis

The analysis of a bearingless rotor system is more involved than that of a hingeless or an articulated rotor. A rigid rotor blade model with equivalent hinge offset and spring, which has been widely used for hingeless and articulated helicopter rotor system analyses, becomes less satisfactory, even for approximate analysis of the bearingless rotor. This is because of the multiple load paths near the blade root and nonlinear bending-torsion couplings resulting from the large twisting motion of the flexbeam. In particular, the bending-torsion couplings are very sensitive to pitch-control configuration parameters and can also vary significantly with changes in the operating conditions. Therefore, all the important structural elements of the bearingless rotor need to be accurately modeled to capture the load redundancies and nonlinear couplings.

In the present study, the UMARC comprehensive aeroelastic analysis code [1] is used to investigate the effects of hub flexbeam damage on the dynamic behavior of the bearingless main rotor system. The finite element/blade element formulation of the UMARC code permits the analysis of bearingless rotor with complex hub configurations involving redundant load paths. Recent applications of the UMARC code for analyzing the dynamics and aeroelastic stability of bearingless rotor helicopters and correlations with test data are available in References 3 and 4. Here, our main efforts are 1) to investigate the dynamic behavior of the bearingless rotor system with a ballistically damaged flexbeam using the UMARC code as the engineering analysis tool, and 2) to evaluate the results in the context of ballistic vulnerability assessment.

1. Formulation

The formulation for the blade and fuselage equations of motion is based on Hamilton's principle [1].

$$\int_{t_1}^{t_2} (\delta U - \delta T - \delta W)\, dt = 0 \tag{1}$$

in which δU, δT and δW are, respectively, the variations in the strain energy, the kinetic energy and the virtual work done by external forces. The expressions for δU and δT are given in Reference 1. The virtual work δW can be expressed as

$$\delta W = \int_0^R (L_u^A \delta u + L_v^A \delta v + L_w^A \delta w + M_\phi^A \delta \phi) dx \tag{2}$$

in which L_u^A, L_v^A, L_w^A and M_ϕ^A are the external aerodynamic loads distributed along the length of the blade in the axial, lead lag, flap and torsion directions, respectively. In the present study, aerodynamic loads are calculated using quasi-steady strip theory. A linear wake model proposed by Drees [5] is used to calculate the rotor inflow distributions. Dynamic stall models are also included to capture some of the unsteady aerodynamic effects.

2. Finite Element Discretization

This section describes the finite element method used in the derivation of the blade-governing equations. In particular, the finite element analysis is used here to remove the spatial dependence from the (blade-governing) equations. To achieve this, the bearingless rotor blades, including flexbeams, torque tubes, and main blades, are discretized into a number of beam elements.

From the Hamiltonian formulation, the integrand of Equation (1) can be expressed as

$$\Delta = \delta U - \delta T - \delta W \ . \tag{3}$$

And in discretized form

$$\Delta = \sum_{i=1}^{n} \Delta_i \tag{4}$$

in which

$$\Delta_i = \delta U_i - \delta T_i - \delta W_i \tag{5}$$

and $\delta U_i, \delta T_i, \delta W_i$ are, respectively, the strain energy, kinetic energy, and virtual work contribution of the ith element, and n is the number of beam elements.

Each beam element has 15 degrees of freedom and consists of two end nodes and three internal nodes (see Figure 2). Each end node has six degrees of freedom which are $u, v, v', w, w', \hat{\phi}$; two internal nodes for the u (axial) degree of freedom; the remaining internal node is for the $\hat{\phi}$ (torsion) degree of freedom. At the element boundary, there is a continuity of displacement for the axial, lag, and flap deflections and twist, and a continuity of slope for the flap and lag bending.

In the formulation, the deflections at any point within an element can be expressed in terms of the shape functions and the nodal degrees of freedom. For the ith element

$$\left\{ \begin{array}{c} u(s) \\ v(s) \\ w(s) \\ \hat{\phi}(s) \end{array} \right\} = \mathbf{H}(s)\ \mathbf{q_e} \tag{6}$$

in which the nodal vector $\mathbf{q_e}$ consists of the 15 degrees of freedom for the beam element, and

$$\mathbf{q_e}^T = \lfloor u_1, u_2, u_3, u_4, v_1, v_1', v_2, v_2', w_1, w_1', w_2, w_2', \hat{\phi}_1, \hat{\phi}_2, \hat{\phi}_3 \rfloor \ . \tag{7}$$

The shape function matrix $\mathbf{H}$ consists of the shape functions for the beam element degrees of freedom and has the form

$$\mathbf{H} = \left[\begin{array}{cccc} H_u^T(s) & \mathbf{0} & \mathbf{0} & \mathbf{0} \\ \mathbf{0} & H_v^T(s) & \mathbf{0} & \mathbf{0} \\ \mathbf{0} & \mathbf{0} & H_w^T(s) & \mathbf{0} \\ \mathbf{0} & \mathbf{0} & \mathbf{0} & H_{\hat{\phi}}^T(s) \end{array} \right] \tag{8}$$

in which the shape function vectors are

$$H_u(s) = \begin{Bmatrix} -4.5s^3 + 9s^2 - 5.5s + 1 \\ 13.5s^3 - 22.5s^2 + 9s \\ -13.5s^3 + 18s^2 - 4.5s \\ 4.5s^3 - 4.5s^2 + s \end{Bmatrix} \tag{9}$$

$$H_v(s) = H_w(s) = \begin{Bmatrix} 2s^3 - 3s^2 + 1 \\ l_i(s^3 - 2s^2 + s) \\ -2s^3 + 3s^2 \\ l_i(s^3 - s^2) \end{Bmatrix} \tag{10}$$

$$H_{\hat{\phi}}(s) = \begin{Bmatrix} 2s^2 - 3s + 1 \\ -4s^2 + 4s \\ 2s^2 - s \end{Bmatrix} . \tag{11}$$

The local spatial coordinate s of the ith element is given by

$$s = \frac{x_i}{l_i}$$

in which l_i is the length of the ith beam element; x_i is the local coordinate of the beam element, and $0 \leq x_i \leq l_i$. The shape functions for the lag and the flap-bending deflection are the Hermitian polynomials which allow the deflections and slopes for the corresponding degrees of freedom to be continuous across the beam element. Since only the continuity of displacement is required for axial deflection and twist, Lagrangian polynomials are used as shape functions for these degrees of freedom.

To preserve the symmetry in the matrices, the virtual displacements $\delta u, \delta v, \delta w$, and $\delta\hat{\phi}$ over the ith element are expressed in the same set of shape functions as

$$\begin{Bmatrix} \delta u(s) \\ \delta v(s) \\ \delta w(s) \\ \delta\hat{\phi}(s) \end{Bmatrix} = \mathbf{H(s)}\ \delta\mathbf{q_e} \tag{12}$$

in which the virtual nodal vector $\delta\mathbf{q_e}$ is the variation of $\mathbf{q_e}$.

Substitution of Equations (6) and (12) into Equation (5) gives

$$\Delta_i = \Delta_i(\mathbf{q_e}, \dot{\mathbf{q}}_\mathbf{e}, \ddot{\mathbf{q}}_\mathbf{e}, \delta\mathbf{q_e}) \ . \tag{13}$$

Following Equation (4), the assembly of the beam elements yields a set of nonlinear ordinary differential equations in terms of the nodal displacements. Let $\mathbf{q}$ denotes the global displacements for the rotor blade and $\delta\mathbf{q}$ the associated global virtual displacements. The global equations can be expressed implicitly as

$$\Delta = \Delta(\mathbf{q}, \dot{\mathbf{q}}, \ddot{\mathbf{q}}, \delta\mathbf{q}) \ . \tag{14}$$

Derivation of the blade-governing equations is completed by applying the geometric boundary conditions to Equation (14). The rotor configuration often dictates the boundary conditions. In case of bearingless rotors, three sets of special boundary conditions are required:

1) Constraints at the in-board end of the torque tube.

2) Compatibility conditions at the junction (clevis) between the flexbeam and the main blade.

3) Root boundary conditions (cantilevered) at the in-board end of the flexbeam.

The in-board end of the torque tube is attached to the pitch link. The in-board end of the main blade is attached to the outboard end of the flexbeam and torque tube through a rigid clevis. This implies that there is continuity of the displacement and bending slopes between two sections of the blade. The cantilevered conditions at the root end of the flexbeam imply that the axial deflection, flap-bending deflection and slope, lag-bending deflection and slope, as well as elastic torsion equal zero.

After applying the boundary conditions, Equation (14) takes the form

$$\Delta = \delta\mathbf{q}^T(\mathbf{M_G}\ddot{\mathbf{q}} + \mathbf{C_G}\dot{\mathbf{q}} + \mathbf{K_G}\mathbf{q} - \mathbf{F_G}) \tag{15}$$

in which $\mathbf{M_G}, \mathbf{C_G}, \mathbf{K_G}$ are the global mass, damping, and stiffness matrices, respectively, and $\mathbf{F_G}$ is the global force vector. Substituting the above equation into Equation (1) and realizing that the blade steady response is periodic for a rotor operating in a steady level flight gives

$$\int_0^{2\pi} \delta\mathbf{q}(\mathbf{M_G}\ddot{\mathbf{q}} + \mathbf{C_G}\dot{\mathbf{q}} + \mathbf{K_G}\mathbf{q} - \mathbf{F_G})\, d\Psi = 0 \ . \tag{16}$$

Note that the above equation has been expressed in terms of the rotor temporal coordinate Ψ.

3. Normal Mode Equations

To reduce computational time, the blade finite element equations are transformed into the normal

mode space using a few coupled natural vibration characteristics. The blade natural vibration modes are obtained by solving an algebraic eigenvalue problem. By neglecting the external loads and the damping matrix, the blade-governing equations can be expressed as

$$\mathbf{M}_{\mathbf{G}}^{\mathbf{s}}\ddot{\mathbf{q}} + \mathbf{K}_{\mathbf{G}}^{\mathbf{s}}\mathbf{q} = \mathbf{0} \ . \tag{17}$$

The solution of (17) is expressed as

$$\mathbf{q} = \bar{\mathbf{q}}e^{i\omega\Psi}$$

Then Equation (17) can be equivalent to the following algebraic eigenvalue problem

$$\omega^2\bar{\mathbf{q}} = (\mathbf{M}_{\mathbf{G}}^{\mathbf{s}})^{-\mathbf{1}}\mathbf{K}_{\mathbf{G}}^{\mathbf{s}}\bar{\mathbf{q}} \tag{18}$$

in which the superscript s denotes structural quantities. These matrices are the inertial and stiffness matrices and are symmetrical. Therefore, this eigenvalue problem can be solved using Jacobi's method [6]. The resulting eigenvalues are real, and the eigenvectors are also real and orthogonal. These eigenvectors represent the blade natural modes, and the square root of the associated eigenvalues represents the blade natural frequencies.

To apply the normal mode transformation, the blade global displacement vector $\mathbf{q}$ is related to the modal displacement vector $\mathbf{p}$ by the normal mode transformation

$$\mathbf{q} = \Phi\,\mathbf{p} \tag{19}$$

in which Φ is an $N_G \times m$ matrix formed with the m blade free vibration modes. Applying the normal mode transformation to Equation (16) results in

$$\int_0^{2\pi} \delta\mathbf{p}\left(\mathbf{M}\ddot{\mathbf{p}} + \mathbf{C}\dot{\mathbf{p}} + \mathbf{K}\mathbf{p} - \mathbf{F}\right) d\Psi = 0 \tag{20}$$

in which

$$\mathbf{M} \ = \ \Phi^T\mathbf{M}_{\mathbf{G}}\Phi$$

$$\begin{aligned} \mathbf{C} &= \Phi^T \mathbf{C_G} \Phi \\ \mathbf{K} &= \Phi^T \mathbf{K_G} \Phi \\ \mathbf{F} &= \Phi^T \mathbf{F_G} \end{aligned} \tag{21}$$

are, respectively, the modal mass, damping, stiffness matrices and load vector. In a forward flight condition, $\mathbf{M}, \mathbf{C}$, and $\mathbf{K}$ contain periodically time-varying coefficients, i.e.,

$$\begin{aligned} \mathbf{M}(\Psi) &= \mathbf{M}(\Psi + 2\pi) \\ \mathbf{C}(\Psi) &= \mathbf{C}(\Psi + 2\pi) \\ \mathbf{K}(\Psi) &= \mathbf{K}(\Psi + 2\pi) \ . \end{aligned}$$

For convenience, all nonlinear terms are put into the load vector $\mathbf{F}$.

4. Finite Element Discretization in Time

In forward flight, the blade modal equations are coupled, nonlinear and contain periodic terms. A finite element in time method based on Hamilton's weak principle is formulated to calculate steady response. The time period for one revolution (i.e., 2 π radians) is discretized into a number of time elements, and within each element there is a polynomial distribution for response. From the assembly of elemental properties, the periodicity of response is imposed by connecting the first and last elements. This yields a set of nonlinear algebraic equations that are solved numerically using a Newton-Raphson procedure. This method is efficient and robust, especially for nonlinear periodic systems.

The blade modal equations, Equation (20), are integrated by parts to yield

$$\int_0^{2\pi} \left\{ \begin{array}{c} \delta \mathbf{p} \\ \delta \dot{\mathbf{p}} \end{array} \right\}^T \left\{ \begin{array}{c} \mathbf{F} - \mathbf{C}\dot{\mathbf{p}} - \mathbf{K}\mathbf{p} \\ \mathbf{M}\dot{\mathbf{p}} \end{array} \right\} d\Psi = \left\{ \begin{array}{c} \mathbf{M}\dot{\mathbf{p}} \\ 0 \end{array} \right\} \Bigg|_0^{2\pi} \ . \tag{22}$$

For a periodic solution, the right-hand side of the above equations is zero, and they can be expressed as

$$\int_0^{2\pi} \delta \mathbf{y}^T \mathbf{Q} \, d\Psi = 0 \tag{23}$$

in which

$$\mathbf{y} = \left\{ \begin{array}{c} \mathbf{p} \\ \dot{\mathbf{p}} \end{array} \right\}$$

and

$$\mathbf{Q} = \left\{ \begin{array}{c} \mathbf{F} - \mathbf{C}\dot{\mathbf{p}} - \mathbf{K}\mathbf{p} \\ \mathbf{M}\dot{\mathbf{p}} \end{array} \right\} . \tag{24}$$

Using the finite element method, the time interval of one rotor revolution of 2π is divided into a number of time elements. It follows that the blade-governing equations are expressed as the sum of the elemental expressions for all the time elements. In particular, Equation (23) takes the form

$$\sum_{i=1}^{N_e} \int_{\Psi_i}^{\Psi_{i+1}} \delta \mathbf{y}_i^T \, \mathbf{Q}_i \, d\Psi = 0 \tag{25}$$

in which $\Psi_1 = 0$, $\Psi_{N_e+1} = 2\pi$, and N_e is the number of time elements being used. The first order Taylor series expansion of Equation (25) about a steady state value of $\mathbf{y}_o = \lfloor \mathbf{p}_o^T \;\; \dot{\mathbf{p}}_o^T \rfloor^T$ is

$$\sum_{i=1}^{N_e} \int_{\Psi_i}^{\Psi_{i+1}} \delta \mathbf{y}_i^T \mathbf{Q}_i(\mathbf{y}_o + \Delta\mathbf{y}) \, d\Psi =$$

$$\sum_{i=1}^{N_e} \int_{\Psi_i}^{\Psi_{i+1}} \delta \mathbf{y}_i^T \left[\mathbf{Q}_i(\mathbf{y}_o) + \mathbf{K}_{ti}(\mathbf{y}_o)\Delta\mathbf{y} \right] d\Psi = 0 \tag{26}$$

in which

$$\mathbf{K}_{ti} = \left[\begin{array}{cc} \frac{\partial \mathbf{F}}{\partial \mathbf{p}} - \mathbf{K} & \frac{\partial \mathbf{F}}{\partial \dot{\mathbf{p}}} - \mathbf{C} \\ \mathbf{0} & \mathbf{M} \end{array} \right]_i . \tag{27}$$

For the *ith* time element, the temporal variation of the modal displacement vector can be expressed in terms of the shape functions and the temporal nodal displacement vector $\boldsymbol{\xi}_i$ as

$$\mathbf{p}_i(\Psi) = \mathbf{H}(s)\boldsymbol{\xi}_i \tag{28}$$

in which the local temporal coordinate s for the *ith* time element is

$$s = \frac{\Psi - \Psi_i}{\Psi_{i+1} - \Psi_i}$$

and $0 \leq s \leq 1$. Note that $\Psi_{i+1} - \Psi_i$ is the time span of the *ith* time element. In Equation (28), $\mathbf{H}(s)$ is the temporal shape function matrix which has the form

$$\mathbf{H} = \lfloor H_1 \mathbf{I}_m, \ldots, H_{n_t+1} \mathbf{I}_m \rfloor$$

in which $\mathbf{I}_m$ is the $m \times m$ identity matrix, and m is the dimension of the modal displacement vector. In the above expression, the subscript n_t refers to the order of the polynomial used in approximating the temporal variation of the modal displacement vector. In particular, if an *nth* order polynomial is used in the approximation, then $n+1$ nodes per degree of freedom are required to completely describe the variation of $\mathbf{p}_i(\Psi)$ within the time element. Therefore, $\mathbf{H}$ is an $m \times m(n_t+1)$ matrix, and $\boldsymbol{\xi}_i$ is an $m(m+1)$ vector.

In the present analysis, fifth order polynomials are used in the approximation, and this results in a total of six nodes for each time element – two end nodes and four internal nodes. The shape functions fall into the Lagrangian polynomial group and are expressed as

$$\begin{aligned}
H_1(s) &= \left(-625s^5 + 1875s^4 - 2125s^3 + 1125s^2 - 274s + 24\right)/24 \\
H_2(s) &= \left(3125s^5 - 8750s^4 + 8875s^3 - 3850s^2 + 600s\right)/24 \\
H_3(s) &= \left(-3125s^5 + 8125s^4 - 7375s^3 + 2675s^2 - 300s\right)/12 \\
H_4(s) &= \left(3125s^5 - 7500s^4 + 6125s^3 - 1950s^2 + 200s\right)/12 \\
H_5(s) &= \left(-3125s^5 + 6875s^4 - 5125s^3 + 1525s^2 - 150s\right)/24 \\
H_6(s) &= \left(625s^5 - 1250s^4 + 875s^3 - 250s^2 + 24s\right)/24 \ .
\end{aligned}$$

With this description, the modal velocity vector can be expressed as

$$\dot{\mathbf{p}}_i = \dot{\mathbf{H}}(\Psi)\, \boldsymbol{\xi}_i \ . \tag{29}$$

In a similar fashion, the expressions for the virtual modal displacement and velocity vector are expressed as

$$\delta \mathbf{p}_i = \mathbf{H}(\Psi) \delta \boldsymbol{\xi}_i \tag{30}$$

$$\delta \dot{\mathbf{p}}_i = \dot{\mathbf{H}}(\Psi) \delta \boldsymbol{\xi}_i \ . \tag{31}$$

Substituting Equations (28) to (31) into Equation (25) yields

$$\sum_{i=1}^{N_e} \int_{\Psi_i}^{\Psi_{i+1}} \delta \boldsymbol{\xi}_i^T \, \mathbf{N}^T \left[\mathbf{Q}_i + \mathbf{K}_{t_i} \mathbf{N}\right] \Delta \boldsymbol{\xi}_i \, d\Psi = 0 \tag{32}$$

in which

$$\mathbf{N} = \left\{ \begin{array}{c} \mathbf{H}(\Psi) \\ \dot{\mathbf{H}}(\Psi) \end{array} \right\} \ . \tag{33}$$

For the periodic solution, the boundary condition for the temporal finite element equations is

$$\mathbf{p}(0) = \mathbf{p}(2\pi) \ . \tag{34}$$

Finally, since the $\delta\boldsymbol{\xi}_i$ are arbitrary for $i = 1, \ldots, N_e$, Equation (32) takes the form

$$\mathbf{Q}^{\mathbf{G}} + \mathbf{K}_t^{\mathbf{G}} \, \Delta\xi^{\mathbf{G}} = \mathbf{0} \tag{35}$$

in which

$$\mathbf{Q}^{\mathbf{G}} = \sum_{i=1}^{N_e} \int_{\Psi_i}^{\Psi_{i+1}} \mathbf{N}^T \mathbf{Q}_i \, d\Psi$$

$$\mathbf{K}_t^{\mathbf{G}} = \sum_{i=1}^{N_e} \int_{\Psi_i}^{\Psi_{i+1}} \mathbf{N}^T \mathbf{K}_{ti} \mathbf{N} \, d\Psi$$

and

$$\Delta\xi^{\mathbf{G}} = \sum_{i=1}^{N_e} \Delta\boldsymbol{\xi}_i \ . \tag{36}$$

Equation (36) is a set of nonlinear algebraic equations and can be solved using the Newton's method. In particular, $\Delta\xi^{\mathbf{G}}$ are solved iteratively, and the subsequent solutions are obtained using

$$\xi^{\mathbf{G}}{}_{i+1} = \xi^{\mathbf{G}}{}_i + \Delta\xi^{\mathbf{G}}{}_i \ . \tag{37}$$

During the iteration process, the vehicle trim controls are also updated according to the coupled trim procedure (for details, see Reference 7).

5. Aeroelastic Analysis

Aeroelastic analysis consists of two phases, vehicle trim and steady response, and is calculated as one coupled solution using a modified Newton method.

Vehicle Trim

Propulsive trim, which simulates the free flight condition of the vehicle, is used to calculate rotor control settings. The solution is determined from vehicle overall equilibrium equations: three force (vertical, longitudinal, and lateral), and three moment (pitch, roll and yaw) equations. For a specified weight coefficient (C_w) and advance ratio (μ), the trim solution calculates the shaft tilt angles (α_s, ϕ_s), the pitch control settings ($\theta_0, \theta_{1c}, \theta_{1s}$), and the tail rotor collective control setting (θ_{tr}). These trim values are calculated iteratively using the modified hub forces and moments including the blade elastic responses.

Steady Response

The steady response involves the determination of time-dependent blade positions at different azimuth locations for one rotor revolution. To reduce computational time, the finite element equations are transformed into normal mode equations, based on the coupled natural vibration characteristics of the blade, as described in Section 3.3. These nonlinear periodic coupled equations are solved for steady response using a finite element in time procedure based on Hamilton's principle in weak form. One rotor revolution is divided into a number of azimuthal elements. The assembly of elements results in nonlinear algebraic equations, which are solved using the Newton-Raphson procedure as described in Section 3.4.

6. Analysis of Damaged Bearingless Rotor System

Most of the comprehensive aeroelastic codes developed to calculate helicopter dynamic response and stability employ the assumption that the response of all the blades is identical with an appropriate phase shift for each blade. Thus, in the rotor response calculation, a set of coupled flap-lag-torsion equations corresponding to a single blade is used. In the study of ballistically damaged rotor system, the motion of each blade has to be represented by an independent set of equations, and their response calculated individually. Otherwise, individual blade can not be represented. This type of solution approach is refered as a

"multi-blade formulation." This formulation also drastically increases the size of equations to be solved. For example, the size of the system equations quadruples for a four-bladed rotor. In the present study, a multi-blade formulation developed in Reference 8 is used to calculate the rotor hub forces and moments. Therefore, the motions of the individual blades are considered in the calculation of hub loads and moments.

Flexbeam Ballistic Damage Model

Ballistic damage to the hub flexbeam is simulated as a reduction in structural capabilities of the affected blade. This is done by reducing the mass, bending, and torsional stiffnesses (m_o, EI_y, EI_z, and GJ) of damaged flexbeam section. These values are estimated based on the prescribed damaged configuration, either observed from ballistic tests or by an analytical method, and used as input to the UMARC code. Since the flexbeam does not contribute to the generation of aerodynamic forces, aerodynamic effects of damage are neglected. However, effects of flexbeam damage on blade aerodynamic loading distributions (i.e., aeroelasticity) are included in the UMARC analysis. The composite damage model used in the present study is constructed in a global sense. It is based on the assumption that ballistic damage to the composite flexbeam, including laminate delaminations, fiber breakages, matrix transverse crackings, and interactional fiber-matrix failures, can be collectively represented as stiffness reductions as well as material discontinuities. More elaborate treatments of individual failure mode of composite materials are available in References 9 and 10. Here, our main efforts are to represent the level of degradation in the composite flexbeam component attributable to ballistic damage and to investigate the effects on overall rotor and helicopter's performance (i.e., $O_{2,3}$ mapping).

7. Solution Procedure

The following procedure was used to study the effects of flexbeam ballistic damage on bearingless rotor blade dynamic response, hub loads, and moments in forward flight conditions.

1) With prescribed input data, vehicle trim equations are calculated using rigid blade flapping (a starting point).

2) Using control inputs from the vehicle trim solution of Step 1) and prescribed blade damage condition,

the blade modal information and rotor nonlinear steady responses are calculated. The results give detailed individual blade responses at different span-wise and azimuthal positions.

3) Hub loads and moments are calculated using elastic rotor responses. Then, the vehicle trim values and blade responses are recalculated iteratively using the modified hub forces and moments. This step is repeated until a converged solution is obtained.

4) Steps 1) to 3) are repeated for different damage configurations.

More details about analysis and results of several case studies, including main rotor blade damages, are reported in References 11 and 12.

IV. Results and Discussion

Numerical results are obtained for a five-bladed soft in-plane bearingless rotor system. Results are first calculated for a undamaged (baseline) rotor configuration. Results then are calculated for this rotor with simulated flexbeam damage conditions, and the effects of damages are assessed. Some important parameters of the rotor used in the present study are given in Table 1.

For the calculation of dynamic response, each rotor blade is discretized into 16 beam elements: 6 for flexbeam, 5 for torque tube, and 5 for main rotor blade (see Figure 3). For normal mode reduction, six coupled rotating natural modes are used, primarily comprised of three flaps, two lags, and one torsion mode. For periodic response, one cycle of time is discretized into eight time elements, and each time element represents a fifth order polynomial distribution of motion.

Table 1: Bearingless Rotor Helicopter Characteristics.

Number of blades, N_b	5
Root cutout, r_c/R	0.3
Mean blade chord, c/R	0.064
Solidity, σ	0.102
Lock number, γ	5.09
Thrust ratio, C_T/σ	0.075
Rotational speed, Ω	355 rpm
Rotating flap natural frequency	1.09/rev
Rotating lag natural frequency	0.65/rev
Rotating torsion natural frequency	5.74/rev

Table 2: BMR Blade Natural Frequencies (per rev).

Mode Number	Baseline	Damage 1	Damage 2
1 (lag)	0.652	0.595	0.562
2 (flap)	1.087	1.081	1.077
3 (coupled)	2.653	3.039	3.059
4 (coupled)	2.934	3.051	4.079
5 (coupled)	5.056	4.897	4.299
6 (torsion)	5.741	5.907	4.998

In the present study, two different flexbeam damage conditions are considered. Damage 1 represents a condition in which the flexbeam suffers 25% reduction in structural capability. Damage 2 represents a more severe damage condition, in which the bending and torsional stiffness of the flexbeam element is further reduced to 50% of the pre-damage values.

Effects of flexbeam damage on the mode shapes of the bearingless main rotor blades are shown in Figures 4 through 12. Since these modes are coupled ones, each flap, lag, and torsional component is shown. For comparison purposes, the results of the baseline (undamaged) case are also shown along with the two damage cases. It is shown that the flexbeam damage affects all the modes of the blade. In particular, the torsional mode is greatly affected by the damage (see Figures 11 and 12). This is because of a large coupling effect between the bending and the torsional modes attributable to the flexbeam. The natural frequencies of the baseline and two damaged cases summarized in Table 2.

From these mode shapes plots, one observes that all components of blade dynamic motions, including flap, lag and torsion, are strongly coupled. It is also interesting to note that this coupling phenomenon, usually observed in higher structural modes, is, with damage, also present in the fundamental mode shapes. For

example, significant torsional components are present in the flap modes. This is thought to be attributable to the bearingless rotor blade design, in which the flexbeam plays a strong role in blade dynamics.

The peak-to-peak amplitudes of structural bendings are shown in Figures 13 through 15 for the undamaged and both damaged cases. Flap bending, lag bending, and torsional moments (nondimensionalized by $m\Omega^2 R^3$) acting on the flexbeam station ($x/R = 0.1$) are shown for three forward flight conditions (advance ratio $\mu = 0.1, 0.2, 0.3$). These moments were calculated using a force summation method. Therefore, they contained all the aeroelastic information of the rotor system, including rotor controls and wake distributions. The damage effects on the flap-bending moments are shown to be large as compared to the lag-bending and torsional moments. One also observes that the peak-to-peak amplitudes of these moments are increased as the vehicle's forward speed increases.

V. Summary

Effects of flexbeam ballistic damage on a soft in-plane bearingless main rotor blade response and loads were investigated using the UMARC comprehensive aeroelastic analysis. The analysis was based on finite element theory in space and time coordinates. The bearingless main rotor (BMR) system, including flexbeams, torque tubes, and main rotor blades, was modeled as a number of elastic beam finite elements, wherein each beam element undergoes flap bending, lag bending, elastic twist, and axial deflections. Aerodynamic forces on rotor blades were calculated using quasi-steady aerodynamic theory with a linear inflow model. Flexbeam ballistic damage was simulated as the changes in the span-wise distribution of mass, bending, and torsional stiffness. Results were calculated for the baseline undamaged rotor system and two hub flexbeam damage conditions.

It was shown that hub flexbeam damage affected all the modes of the blade, and these effects were more distinct in the higher modes. It was also found that the bending-torsion coupling effects were quite significant in the bearingless rotor dynamics.

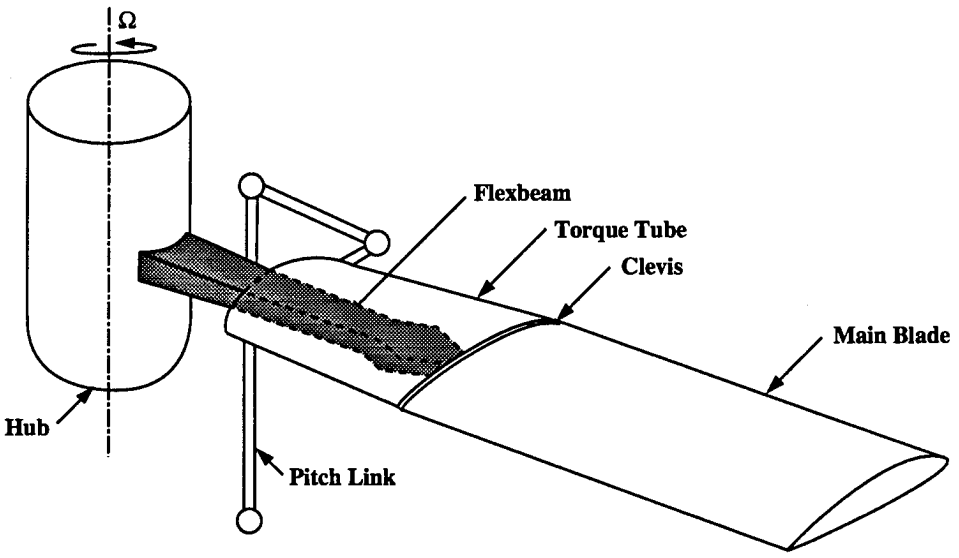

FIGURE 1.—*Schematic of Bearingless Main Rotor (BMR) System.*

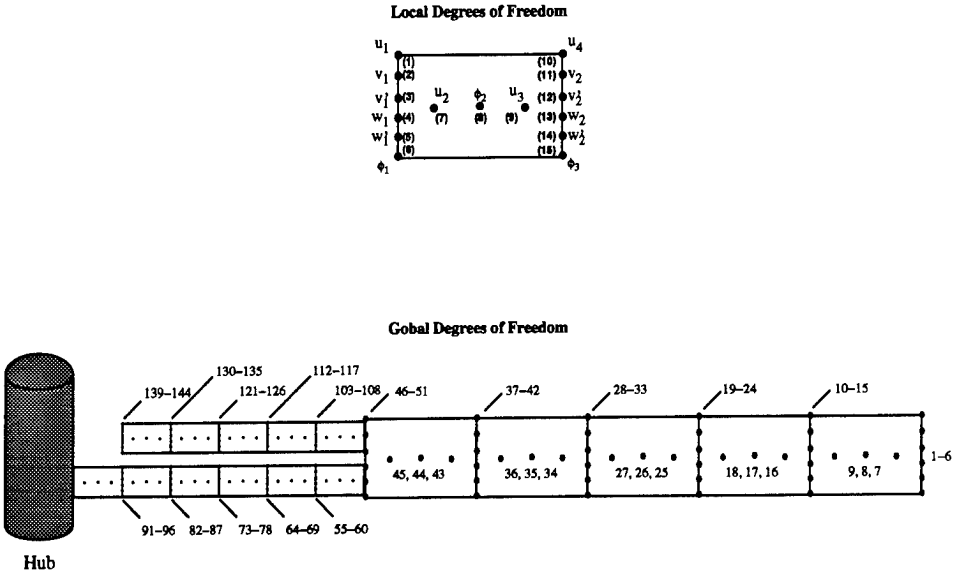

Figure 2: Local and Global Degress of Freedom of BMR Blade.

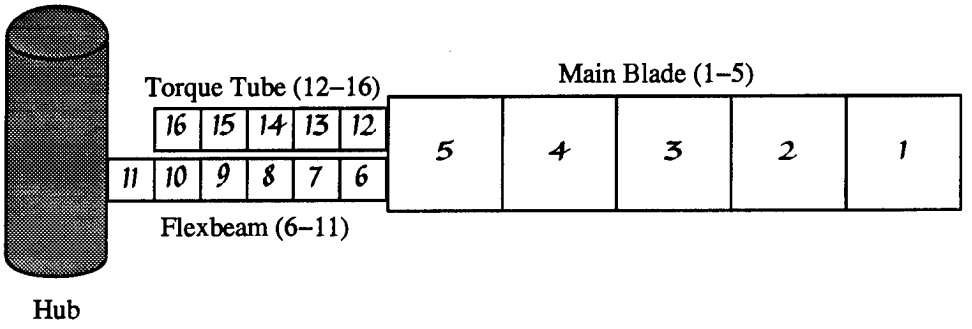

Figure 3: Finite Element Model of Bearingless Main Rotor.

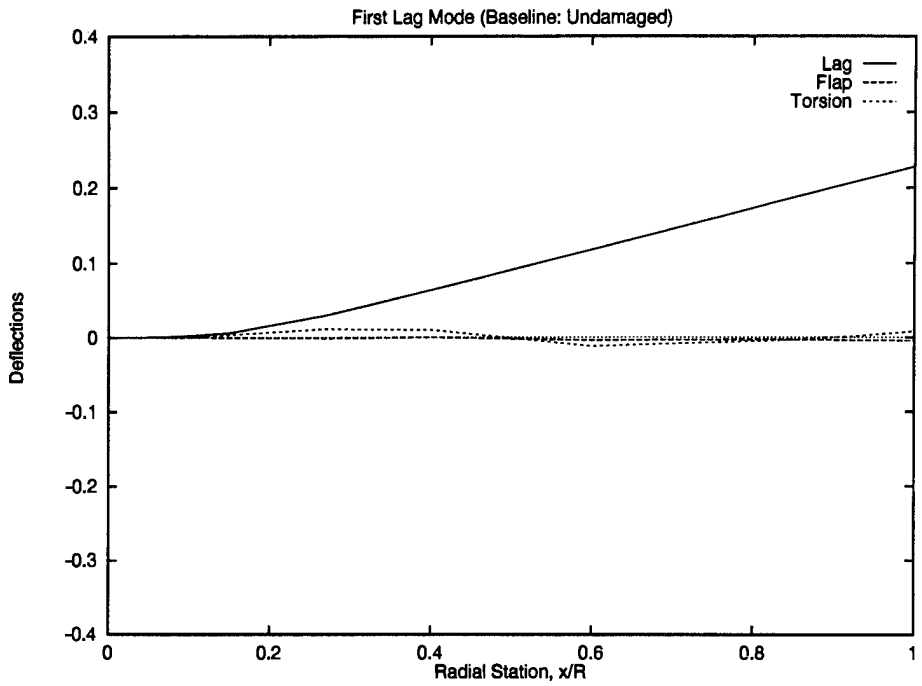

Figure 4: Lag Mode of Baseline Blade (Undamaged).

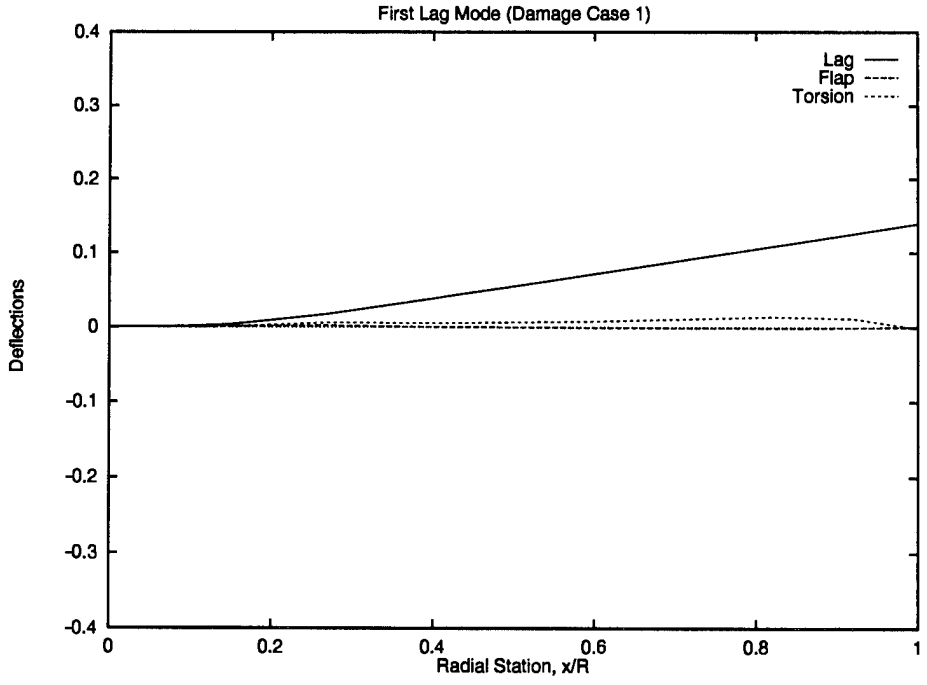

Figure 5: Lag Mode of Damaged Flexbeam Blade (Case 1).

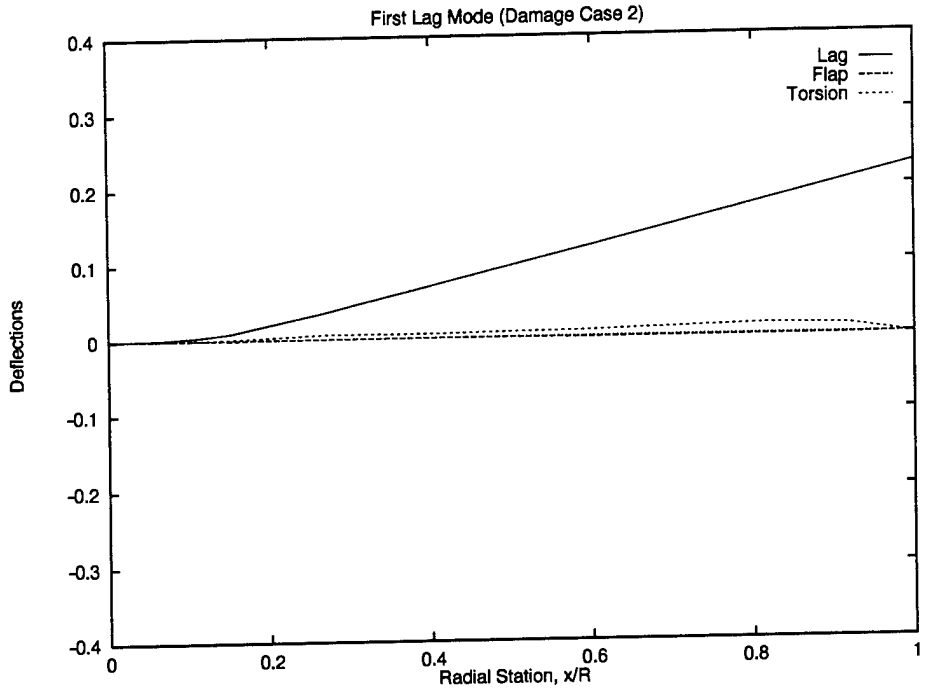

Figure 6: Lag Mode of Damaged Flexbeam Blade (Case 2).

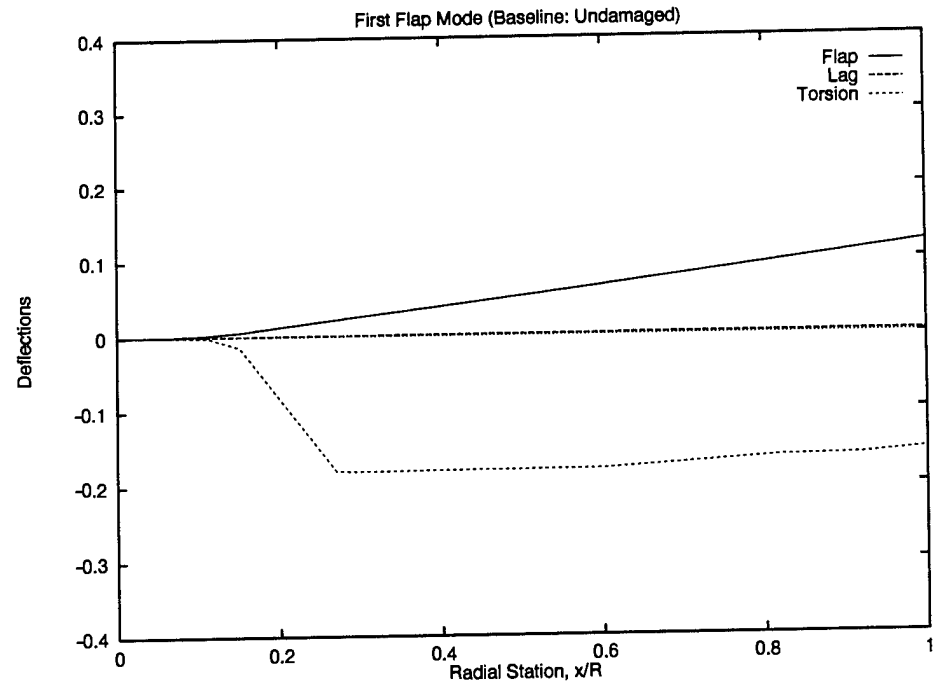

Figure 7: Flap Mode of Baseline Blade (Undamaged).

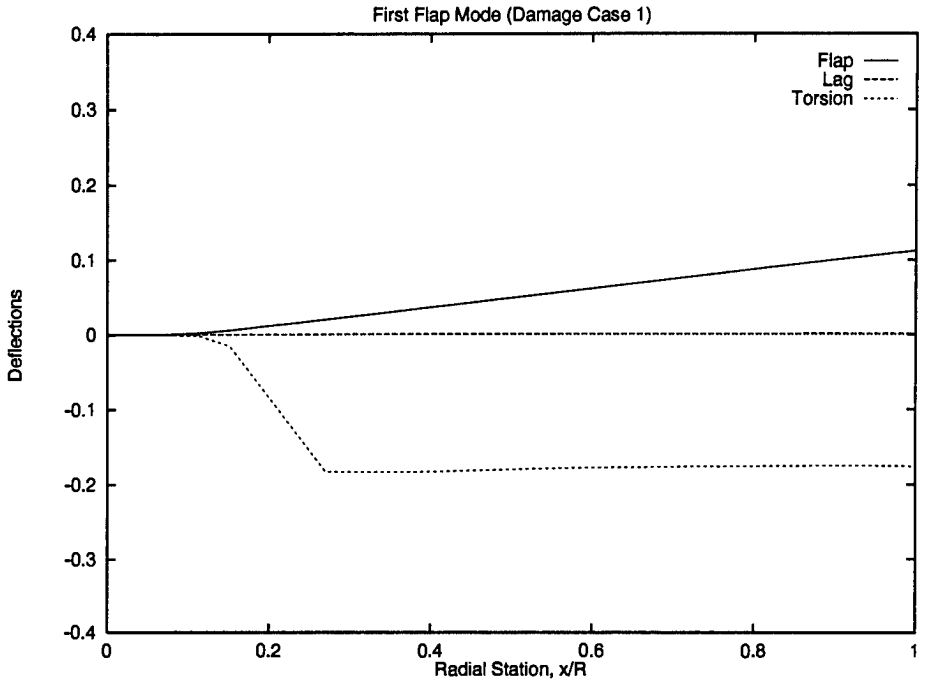

Figure 8: Flap Mode of Damaged Flexbeam Blade (Case 1).

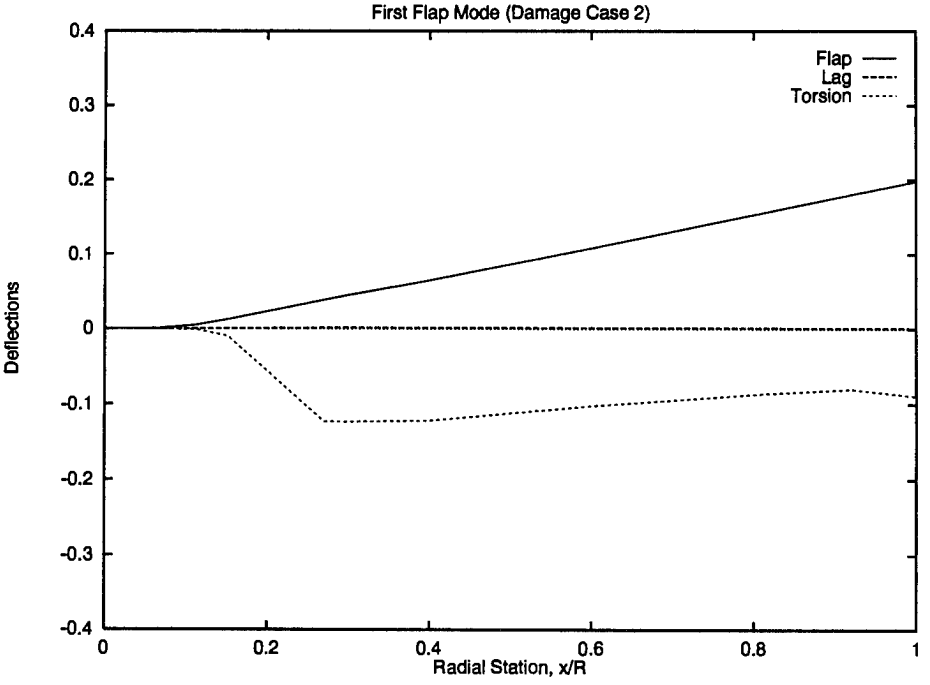

Figure 9: Flap Mode of Damaged Flexbeam Blade (Case 2).

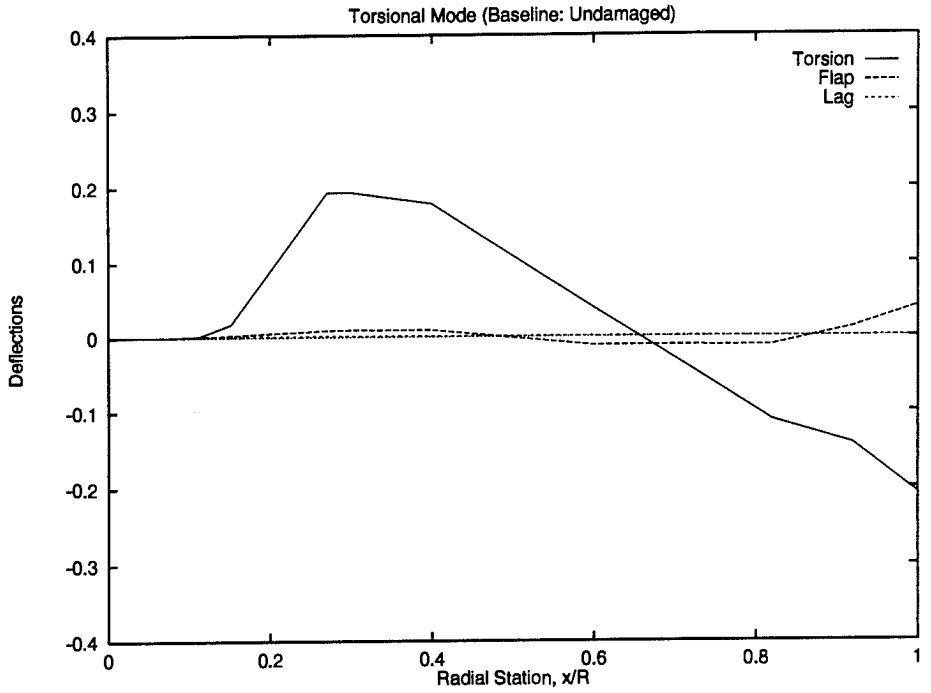

Figure 10: Torsion Mode of Baseline Blade (Undamaged).

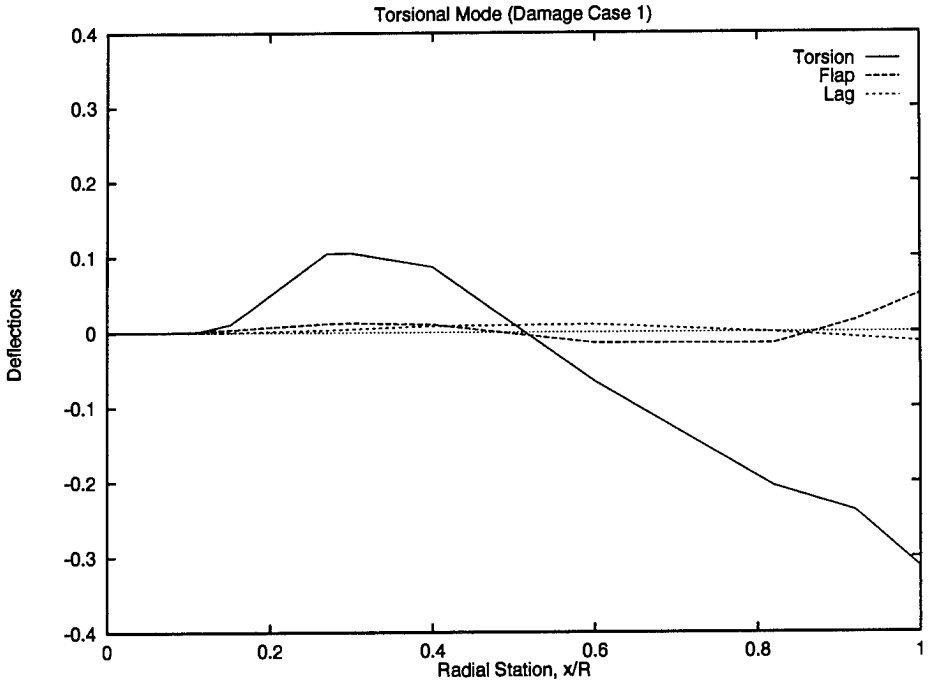

Figure 11: Torsion Mode of Damaged Flexbeam Blade (Case 1).

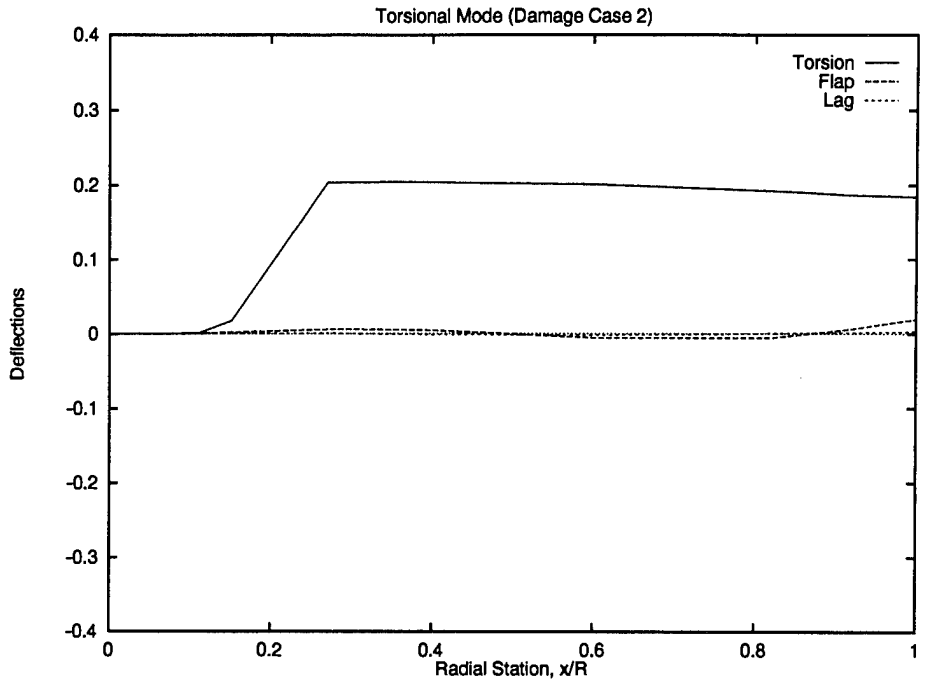

Figure 12: Torsion Mode of Damaged Flexbeam Blade (Case 2).

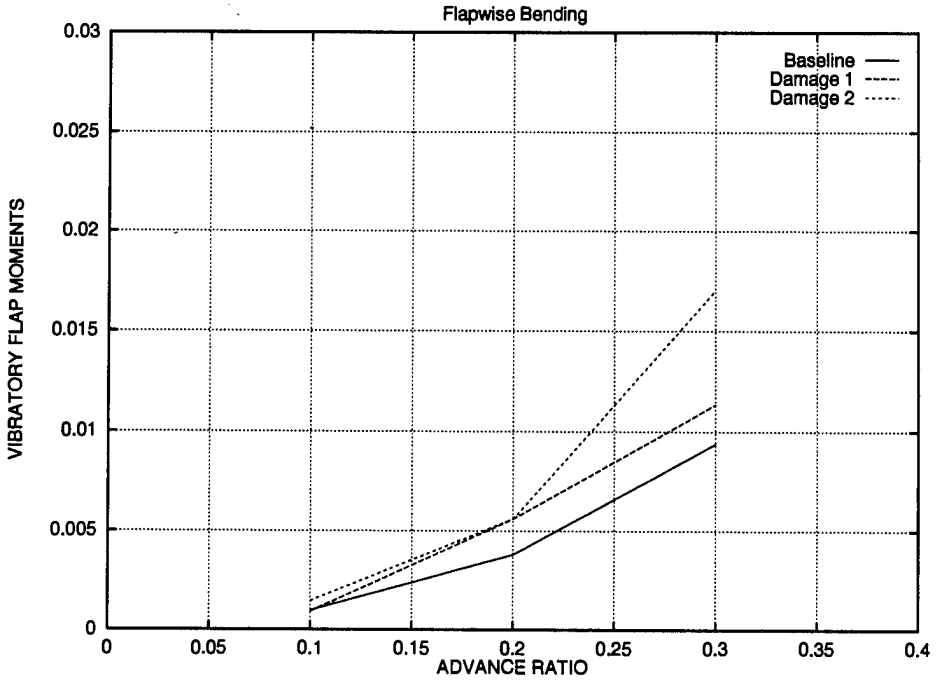

Figure 13: Effects of Flexbeam Damage on Flap-Bending Moments at .1R.

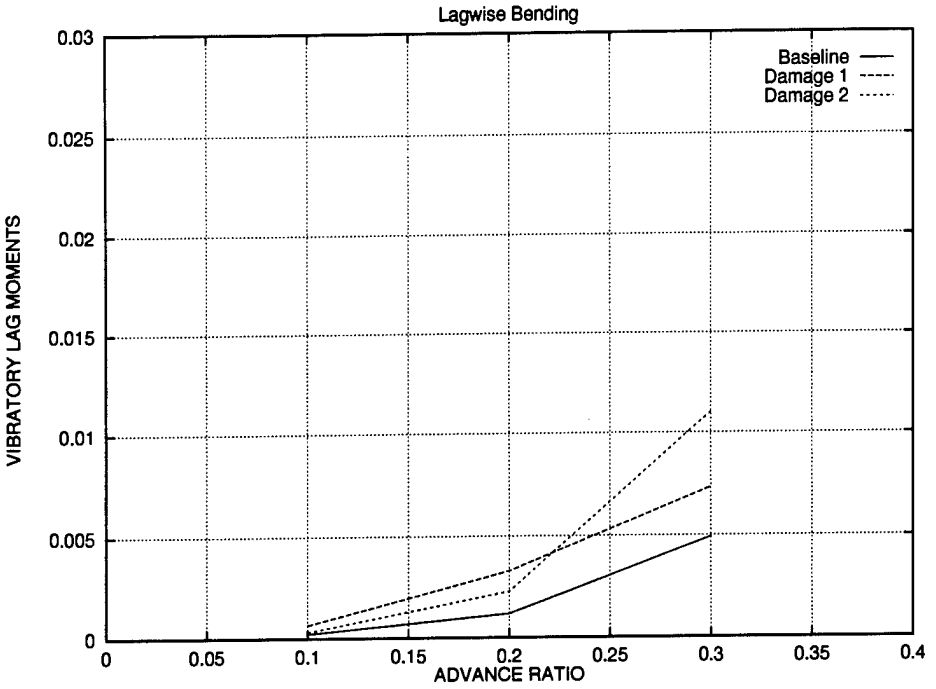

Figure 14: Effects of Flexbeam Damage on Lag-Bending Moments at .1R.

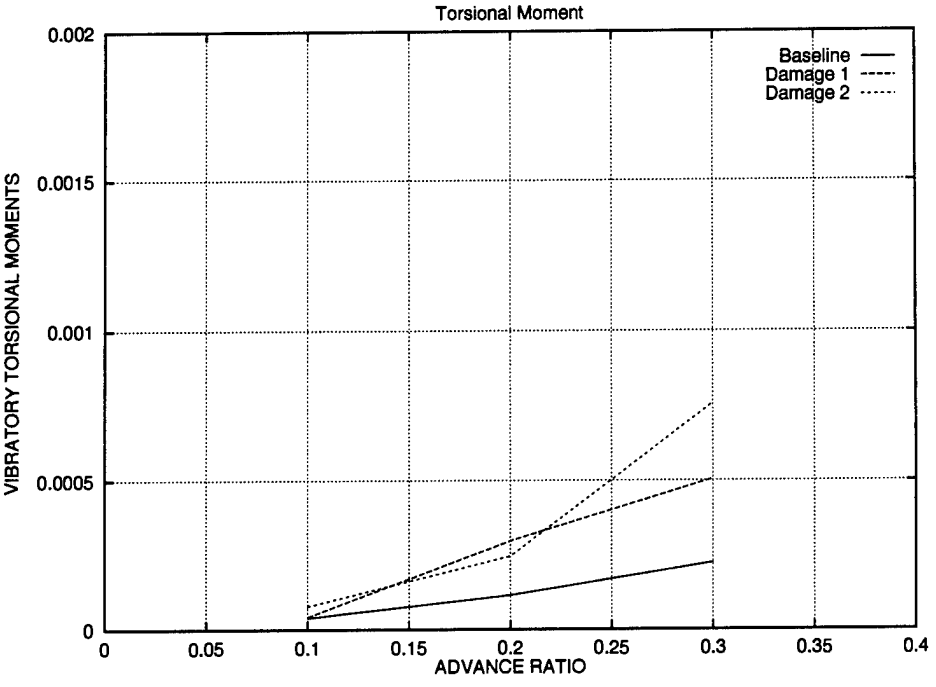

Figure 15: Effects of Flexbeam Damage on Torsional Moments at .1R.

VI. References

[1] Bir, G., I. Chopra, and K. C. Kim *et al.* "University of Maryland Advanced Rotorcraft Code (UMARC): Theory Manual." Technical Report 92-02, Aerospace Engineering Department, University of Maryland, College Park, MD, May 1992.

[2] Walbert, J. N., L. Roach, and M. Burdeshaw. "Current Directions in the Vulnerability/Lethality Process Structure." Army Research Laboratory Technical Report, ARL-TR-296, Aberdeen Proving Ground, MD, October 1993.

[3] Nguyen, K. *et al.* "Aeroelastic Stability of the McDonnell Douglas Advanced Bearingless Rotor." *Proceedings of the American Helicopter Society's (AHS) 49th Annual Forum*, St. Louis, MO, May 1993.

[4] Wang, J., J. Duh, and J. S. Fuh. "Stability of the Sikorsky S-76 Bearingless Main Rotor." *Proceedings of the American Helicopter Society's (AHS) 49th Annual Forum*, St. Louis, MO, May 1993.

[5] Drees, J. "A Theory of Airflow Through Rotors and its Application to Some Helicopter Problems." Journal of the Helicopter Association of Great Britain, Vol. 3, March 1949.

[6] Wilkinson, J. The Algebraic Eigenvalue Problems, London: Oxford University Press, 1965.

[7] Kim, K. C. "Helicopter Trim Calculation in Forward Flight." *Proceedings of the Summer Computer Simulation Conference*, Society for Computer Simulation (SCS), Boston, MA, July 1993.

[8] Chopra, I. "Helicopter Dynamics and Aeroelasticity." Technical Notes, Center for Rotorcraft Education and Research, Aerospace Engineering Department, University of Maryland, College Park, MD, January 1991.

[9] O'Brien, T. K. "Characterization of Delamination Onset and Growth in a Composite Laminate." Damage in Composite Materials, ASTM STP No. 775, American Society for Testing and Materials, 1982.

[10] Highsmith, A. L. and K. L. Reifsnider. "Stiffness-Reduction Mechanism in Composite Laminate." Damage in Composite Materials, ASTM STP No. 775, American Society for Testing and Materials, 1982.

[11] Kim, K. C. "Blade and Hub Loads of Ballistically Damaged Helicopter Rotors." Army Research Laboratory Technical Report, ARL-TR-235, Aberdeen Proving Ground, MD, October 1993.

[12] Kim, K. C. "Vulnerability Assessment Process for Helicopter Rotor System with Damage." Paper presented at the American Defense Preparedness Association's (ADPA) Testing for Combat Survivability Symposium, Gaithersburg, MD, May 1994.

NO. OF COPIES	ORGANIZATION
2	DEFENSE TECHNICAL INFO CTR ATTN DTIC DDA 8725 JOHN J KINGMAN RD STE 0944 FT BELVOIR VA 22060-6218
1	DIRECTOR US ARMY RESEARCH LAB ATTN AMSRL OP SD TA 2800 POWDER MILL RD ADELPHI MD 20783-1145
3	DIRECTOR US ARMY RESEARCH LAB ATTN AMSRL OP SD TL 2800 POWDER MILL RD ADELPHI MD 20783-1145
1	DIRECTOR US ARMY RESEARCH LAB ATTN AMSRL OP SD TP 2800 POWDER MILL RD ADELPHI MD 20783-1145
	ABERDEEN PROVING GROUND
5	DIR USARL ATTN AMSRL OP AP L (305)

NO. OF COPIES ORGANIZATION

1 OSD OUSD AT
STRT TAC SYS
ATTN DR SCHNEITER
3090 DEFNS PENTAGON RM 3E130
WASHINGTON DC 20301-3090

1 ODDRE AT
ACQUISITION AND TECH
ATTN DR GONTAREK
3080 DEFENSE PENTAGON
WASHINGTON DC 20310-3080

1 ASST SECY ARMY RESEARCH
DEVELOPMENT ACQUISITION
ATTN SARD ZD RM 2E673
103 ARMY PENTAGON
WASHINGTON DC 20310-0103

1 ASST SECY ARMY RESEARCH
DEVELOPMENT ACQUISITION
ATTN SARD ZP RM 2E661
103 ARMY PENTAGON
WASHINGTON DC 20310-0103

1 ASST SECY ARMY RESEARCH
DEVELOPMENT ACQUISITION
ATTN SARD ZS RM 3E448
103 ARMY PENTAGON
WASHINGTON DC 20310-0103

1 ASST SECY ARMY RESEARCH
DEVELOPMENT ACQUISITION
ATTN SARD ZT RM 3E374
103 ARMY PENTAGON
WASHINGTON DC 20310-0103

1 UNDER SEC OF THE ARMY
ATTN DUSA OR
RM 2E660
102 ARMY PENTAGON
WASHINGTON DC 20310-0102

1 ASST DEP CHIEF OF STAFF
OPERATIONS AND PLANS
ATTN DAMO FDZ RM 3A522
460 ARMY PENTAGON
WASHINGTON DC 20310-0460

1 DEPUTY CHIEF OF STAFF
OPERATIONS AND PLANS
ATTN DAMO SW RM 3C630
400 ARMY PENTAGON
WASHINGTON DC 20310-0400

NO. OF COPIES ORGANIZATION

1 ARMY RESEARCH LABORATORY
ATTN AMSRL ST
DR FRASIER
2800 POWDER MILL RD
ADELPHI MD 20783-1197

1 ARMY RESEARCH LABORATORY
ATTN AMSRL SL
DR WADE
WSMR NM 88002-5513

1 ARMY RESEARCH LABORATORY
ATTN AMSRL SL E
MR MARES
WSMR NM 88002-5513

1 ARMY TRADOC ANL CTR
ATTN ATRC W
MR KEINTZ
WSMR NM 88002-5502

1 ARMY TRNG & DOCTRINE CMND
ATTN ATCD B
FT MONROE VA 23651

ABERDEEN PROVING GROUND

1 CDR USATECOM
ATTN: AMSTE-TA

2 DIR USAMSAA
ATTN: AMXSY-ST
AMXSY-D

4 DIR USARL
ATTN: AMSRL-SL, J WADE (433)
AMSRL-SL-I, M STARKS (433)
AMSRL-SL-C, W HUGHES (E3331)
AMSRL-SL-B, P DEITZ (328)

NO. OF COPIES	ORGANIZATION
2	DAVID TAYLOR RESEARCH CENTER ATTN DR DAVID HASS MR JOHN VORWALD SYSTEMS DEPARTMENT CODE 127 BETHESDA MD 20084-5000
	ABERDEEN PROVING GROUND
20	DIR USARL ATTN: AMSRL-SL-BA, DR. K. KIM

INTENTIONALLY LEFT BLANK.

USER EVALUATION SHEET/CHANGE OF ADDRESS

This Laboratory undertakes a continuing effort to improve the quality of the reports it publishes. Your comments/answers to the items/questions below will aid us in our efforts.

1. ARL Report Number ARL-TR-921 Date of Report January 1996

2. Date Report Received _____

3. Does this report satisfy a need? (Comment on purpose, related project, or other area of interest for which the report will be used.) _____

4. Specifically, how is the report being used? (Information source, design data, procedure, source of ideas, etc.) _____

5. Has the information in this report led to any quantitative savings as far as man-hours or dollars saved, operating costs avoided, or efficiencies achieved, etc? If so, please elaborate. _____

6. General Comments. What do you think should be changed to improve future reports? (Indicate changes to organization, technical content, format, etc.) _____

CURRENT ADDRESS

_____
Organization

_____
Name

_____
Street or P.O. Box No.

_____
City, State, Zip Code

7. If indicating a Change of Address or Address Correction, please provide the Current or Correct address above and the Old or Incorrect address below.

OLD ADDRESS

_____
Organization

_____
Name

_____
Street or P.O. Box No.

_____
City, State, Zip Code

(Remove this sheet, fold as indicated, tape closed, and mail.)
(DO NOT STAPLE)

DEPARTMENT OF THE ARMY

OFFICIAL BUSINESS

NO POSTAGE
NECESSARY
IF MAILED
IN THE
UNITED STATES

BUSINESS REPLY MAIL
FIRST CLASS PERMIT NO 0001,APG,MD

POSTAGE WILL BE PAID BY ADDRESSEE

DIRECTOR
U.S. ARMY RESEARCH LABORATORY
ATTN: AMSRL-SL-BA
ABERDEEN PROVING GROUND, MD 21005-5068